Observer based extremum seeking control for cell population models with uncertain growth dynamics

P. Jerono [*] **M. Guay** [**] **T. Meurer** [*]

[*] *Digital Process Engineering Group (DPE), Karlsruhe Institute of Technology, Karlsruhe, Germany*
[**] *Department of Chemical Engineering, Queen's University, Kingston, Ontario, Canada*

Abstract: In this work the optimal control problem of maximizing the cell production rate in chemostat reactors by manipulating the dilution rate under possibly time–varying uncertainties in the growth rate is addressed. Considering that the cell mass distribution is not an available measurement during cultivation, three estimation problems are formulated and addressed. Based on the respective observability property of each subsystem, extended Kalman filters are designed for the estimation of the gradient with respect to the input, uncertainties in the growth rate, and the cell mass distribution density function based on biomass measurements. Finally, the convergence of the proposed observers and optimal control strategy is tested in simulations.

Keywords: Cell population dynamics; Uncertain systems; Observer design; Extremum seeking.

---

1. INTRODUCTION

The interest of cell population distributions in biological systems has increased considerably in the last few decades (Ramkrishna and Singh, 2014). This is due to the development of modern sensors such as flow cytometry for the measurement of cell distributions and the fact that different metabolic and product formation pathways of biological cultures are often related to their respective cell stage. The number of cells within these stages can be represented by cell size, mass or age distributions. Mathematically, these structured cell population dynamics can be described by cell population balance models, which usually consist of a partial integro–differential equation that is coupled to a set of ordinary differential equations to account for nutrient dynamics. These types of models have successfully been utilized to design nonlinear model–based control schemes in a simulative environment (Sharifian and Fanaei, 2008; Kurth et al., 2021) and for control and observer design in an experimental lab–scale reactor of yeast fermentation (Jerono et al., 2021a, 2022).

A big challenge when these models are utilized for the control of real processes is the regulation and mutational adaptation of the cells in long–term cultivations, which are documented for several species (see, e.g., Ferenci (2007)). In a lab–scale yeast fermentation chemostat experiment, it turned out that a stabilizing feedback controller is crucial for maintaining the control target of a desired cell density distribution (Jerono et al., 2022). This becomes most relevant when the control target is to drive the system to an optimal operation point, like a maximum cell production rate, which might be a priori unknown and also might change over time. Due to the stochastic nature of biological diversity and mutational adaptation, the quantization of these effects is difficult and might not be repeatable between experiments. Therefore, it is convenient to consider model–free optimization control schemes like extremum seeking and its partly model–free variations (Ariyur and Krstic, 2003; Guay et al., 2004; Guay and Dochain, 2015).

Additional challenges arise, when the objective function is not directly measured, which requires to integrate an observer operating on available measurements in the control strategy. The observer design and its convergence typically rely on the observability property with respect to the process dynamics by means of a mathematical model and the available measurements during cultivation. When the process dynamics are additionally uncertain, the questions arise if these uncertainties can also be estimated by a feasible observer design and what is their impact on the estimation of the objective function.

In this work the optimal control problem of maximizing the cell production rate in chemostat reactors under the effect of possibly time–varying uncertainties in the growth rate by manipulating the dilution rate is addressed. The main idea is to separate the estimation of the cell distribution and uncertainties in growth from the optimal control problem, which can also be formulated as an estimation problem in terms of estimating an unknown gradient. Based on the analysis of the observability property of the considered subsystems, extended Kalman filters are designed to estimate the cell distribution density function, estimate possibly time–varying uncertainties in the growth dynamics and to drive the system to optimal operation conditions by means of the cell production rate in chemostat operation.

[⋆] This work is partially supported by funding from the the Mitacs Globalink Research Award (GRA) IT38080.

2. MODEL FORMULATION

Consider the cell population balance equation

$$\begin{aligned}\partial_t n(m,t) &= -\partial_m[r(m,s)n(m,t)] - \Gamma(m,s)n(m,t)\\ &\quad + 2\int_m^{m^*}\Gamma(\mu,s)p(m,\mu)n(\mu,t)\mathrm{d}\mu \\ &\quad - Dn(m,t) \\ n(m^*,t) &= 0, \quad n(m,0) = n_0(m)\end{aligned} \tag{1a}$$

in chemostat operation with the dilution rate $D \neq 0$. Furthermore, $t \in \mathbb{R}_{\geq 0}$ is the time and $m \in [m_*,\, m^*]$ is the cell mass with its minimum and maximum given by m_* and m^*, respectively. The cell mass distribution density function is given by $n(m,t) : [m_*,\, m^*] \times \mathbb{R}_{\geq 0} \to \mathbb{R}_{\geq 0}$ and the cell growth rate is denoted as $r(m,s) : [m_*,\, m^*] \times \mathbb{R}_{\geq 0} \to \mathbb{R}_{\geq 0}$ with the substrate concentration $s \in \mathbb{R}_{\geq 0}$. The cell division rate is given by $\Gamma(m,s) : [m_*,\, m^*] \times \mathbb{R}_{\geq 0} \to \mathbb{R}_{\geq 0}$ and $p(m,\mu) : [m_*,\, m^*] \times [m_*,\, m^*] \to \mathbb{R}_{\geq 0}$ is the division probability density function, which determines the possibility that a mother cells of mass μ produces daughter cells of mass m by division. In virtue of its definition, $p(m,\mu)$ fulfills the property

$$p(m,\mu) = 0\,, \quad \forall \mu \leq m.$$

According to Mantzaris and Daoutidis (2004); Jerono et al. (2021b) it is chosen as a symmetric binomial distribution

$$p(m,\mu) = \frac{1}{B(q)}\frac{1}{\mu}\left(\frac{m}{\mu}\right)^{q-1}\left(1-\frac{m}{\mu}\right)^{q-1},$$

where $B(q)$ denotes the normalization factor given by the symmetric Beta distribution

$$B(q) = \frac{2\Gamma_f(q)}{\Gamma_f(2q)},$$

and the cell division rate $\gamma(m)$ is given by a ramp function

$$\gamma(m) = \begin{cases} 0, & \text{if } m \leq \bar{m} \\ \beta m, & \text{if } m > \bar{m}, \end{cases}$$

with a constant slope β and $\bar{m}$ denotes the minimum cell mass required for division.

To take into account the substrate dynamics, the cell population balance equation is coupled with

$$\dot{s} = -\int_{m_*}^{m^*} r(m,s)n(m,t)\mathrm{d}m + D\left(s_{\text{in}} - s\right), \tag{1b}$$

where s_{in} denotes the substrate inlet concentration. Combining (1a) and (1b) the model is given by a partial integro-differential equation coupled with a ordinary nonlinear differential equation accounting for the substrate dynamics. Further, it is considered that growth is proportional to mass and division is proportional to growth, i.e.,

$$r(m,s) = \rho(s)m, \qquad \Gamma(m,s) = \gamma(m)\rho(s)$$

and $\rho(s)$ is given by the Monod growth rate

$$\rho(s) = k_s\frac{s}{K_s + s}. \tag{2}$$

Recalling mass conservation, i.e., that by division cell mass is not lost nor produced, it holds that

$$\int_{m_*}^{m^*} m\Gamma(m,s)n(m,t)\mathrm{d}m = \int_{m_*}^{m^*} 2m\left(\int_{m_*}^{m^*}\Gamma(\mu,s)p(m,\mu)n(m,t)\mathrm{d}\mu\right)\mathrm{d}m\,.$$

Determining the first moment of the cell population balance equation (1a) leads to

$$b = \int_{m_*}^{m^*} mn(m,t)\mathrm{d}m \tag{3}$$

with b given by the total biomass and further one obtains

$$\dot{b} = \rho(s)\int_{m_*}^{m^*} mn(m,t)\mathrm{d}m = \rho(s)b. \tag{4}$$

Note that in terms of the total biomass dynamics the model equations (1) can also be written as

$$\dot{b} = \rho(s)b - Db \tag{5a}$$

$$\dot{s} = -\rho(s)b + D\left(s_{\text{in}} - s\right), \tag{5b}$$

so that the solution of the biomass in the mass balance model (5) corresponds to the solution of the first moment of the cell distribution following the dynamics (1a).

The system measurement is given by the first moment of the cell distribution density function, i.e.,

$$y = \int_{m_*}^{m^*} mn(m,t)\mathrm{d}m = b\,, \tag{6}$$

and the objective function for optimization is considered to be total biomass production rate in the operation points of chemostat cultivation, i.e.,

$$\max_D J(D) = \max_D \int_{m_*}^{m^*} mn(m,t)\mathrm{d}mD \tag{7}$$

with the input given by the dilution rate D. Note that in chemostat operation ($D \neq 0$) the cell distribution density function $n(m,t)$ also depends on D although this dependency is not explicitly highlighted here.

Furthermore, it is assumed that the real process is subject to time–varying uncertainties in the growth rate due to mutational adaptation of the cells to the environment. This behavior is typically present in long–term chemostat cultivations and documented for several species (see, e.g., (Ferenci, 2007)). A crucial aspect of these uncertainties is given by the fact that the nature and impact are usually unknown in advance. Here, it is considered that the time–varying uncertainty ϵ appears in the maximum growth rate k_s in terms of

$$\bar{\rho}(s,\epsilon) = (k_s + \epsilon)\frac{s}{s + K_s}\,. \tag{8}$$

Technically, the mutual adaptation can also lead to changes in the half saturation constant K_s, or even to increased or decreased inhibition effects, which are assumed not to be present in the given process. Since the unknown impact of the mutual adaptation gives an additional layer of uncertainty, it is proposed to decouple the corresponding estimation problem from the optimal control problem which is discussed in the next section.

3. SEPARATION OF THE ESTIMATION PROBLEMS

Based on the previous considerations, three estimation problems are addressed. One is given by estimating the cell distribution density function, namely $\hat{n}(m,t)$, based on online available biomass measurements taking the cell population model (1) into account. The second estimation problem consists of estimating uncertainties in the growth rate, namely $\hat{\epsilon}$, also based on biomass measurements taking into account the mass balance model (5). Finally, the last estimation problem is given by estimating the gradient of the considered cost functional (9), which is derived in this section. Note that in general these estimation problems are not decoupled because the uncertainties in the growth rate directly couple into estimation the cell distribution density and also have an impact on the gradient estimation. Nevertheless, the estimation of the uncertainties in the growth kinetics are not required for the gradient estimation when a model free estimation approach is chosen for the extremum seeking controller. In this case, the gradient estimation can be decoupled from the other estimation problems. This separation is in particular advantageous when the nature and magnitude of the uncertainties are unknown. In the following the process models for the observers of the given estimation problems are derived.

3.1 Observer based extremum seeking controller

Extremum seeking control techniques have proven to be suitable for the optimal control of uncertain dynamics. Although the underlying idea of the concept is rather old (Leblanc, 1922), it has been modified and improved with respect to various properties under certain assumptions (see, e.g., Ariyur and Krstic (2003); Guay et al. (2004); Guay and Dochain (2015)).

In this work an observer based extremum seeking control strategy is proposed similar to the one presented in Gelbert et al. (2012); Lutz et al. (2019). The technique relies on estimating the gradient of an a priori unknown but measured cost function, which is assumed, given a feasible separation of the time scales, to behave like a static map with respect to the system input. The schematic sketch of the controller is shown in Fig. 1 where $d(t)$ denotes a zero mean dither signal.

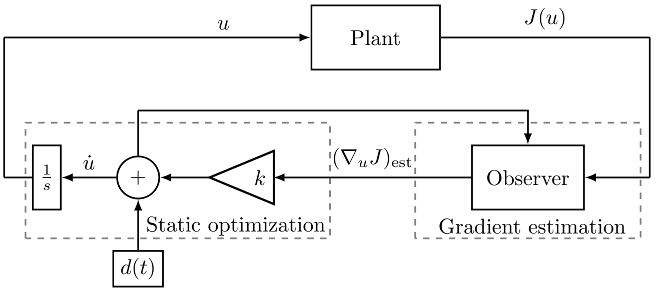

Fig. 1. Schematic sketch of the extremum seeking controller with observer based gradient estimation.

Consider the measurement of an unknown static cost function

$$y = J(u) \tag{9}$$

driven by the input u. The time derivative of (9) then reads

$$\dot{J}(u) = \frac{\partial}{\partial u} J(u) \dot{u} \,. \tag{10}$$

Introducing the state vector $\boldsymbol{x} = \left[J(u),\, \frac{\partial}{\partial u} J(u)\right]^{\mathrm{T}}$, equation (10) can be written as

$$\dot{x}_1 = x_2 \dot{u} \,. \tag{11}$$

Clearly, the time derivative of x_2, namely the gradient with respect to u, is unknown so that its process model is assumed to be driven by a Gaussian random process $w \sim \mathcal{N}(0, q)$. By this assumption the state space equations read

$$\dot{\boldsymbol{x}} = \begin{bmatrix} 0 & \dot{u} \\ 0 & 0 \end{bmatrix} \boldsymbol{x} + \begin{bmatrix} 0 \\ w \end{bmatrix}, \tag{12}$$

which are linear, but time–variant due to $\dot{u}$. Note that according to Fig. 1 the time derivative of the input is given by

$$\dot{u} = k x_2 + d \,.$$

Therefore, the resulting state space equations read

$$\dot{x}_1 = x_2 (k x_2 + d) \tag{13a}$$

$$\dot{x}_2 = w \tag{13b}$$

and represent a nonlinear, time–variant system.

An alternative process model is obtained when the dither signal is added after the integrator instead of before in Fig. 1. By this modification one obtains

$$u = \int_{t_0}^{t} k \frac{\partial}{\partial u} J(u) \mathrm{d}\tau + d + u_0 = \int_{t_0}^{t} k x_2(\tau) \mathrm{d}\tau + d + u_0 \,.$$

The time derivative of the input signal reads

$$\dot{u} = k x_2 + \dot{d} \,.$$

The process model of the unknown cost function is then given by

$$\dot{x}_1 = x_2 \left(k x_2 + \dot{d} \right) \tag{14a}$$

$$\dot{x}_2 = w \tag{14b}$$

and depends, in contrast to (13), on the time derivative of the dither signal. Nevertheless, in this work the dither signal is passed before the integrator. An advantage of this variant becomes clear when investigating the observability property of the given process model for gradient estimation which is addressed in Section 4. It is worth to mention that the proposed extremum seeking control scheme does not stabilize a possible unstable optimum. Therefore, it is necessary that the plant dynamics are stable, which holds true for the operation points of bioreactors following Monod kinetics in chemostat operation.

3.2 Growth rate disturbance process model

The process model for estimating uncertainties in growth dynamics can be derived as follows. Let ϵ denote an unknown function in the growth dynamics such that the total biomass growth rate reads

$$\bar{\rho}(s, \epsilon) = (k_s + \epsilon) \frac{s}{K_s + s} \,.$$

Note that depending on $\bar{\rho}(s, \epsilon)$ it is possible to estimate ϵ and s jointly based on biomass measurements. To illustrate this in Section 4 consider the state vector $\boldsymbol{x}_b = [b,\, s,\, \epsilon]$ and the process model

$$\begin{aligned} \dot{b} &= \bar{\rho}(s, \epsilon) b - D b \\ \dot{s} &= -\bar{\rho}(s, \epsilon) b - D(s - s_{\mathrm{in}}) \\ \dot{\epsilon} &= w_\rho \\ y &= b, \end{aligned} \tag{15}$$

where it is assumed that the dynamics of the unknown function ϵ are driven by a Gaussian random process $w_\rho \sim \mathcal{N}(0, q_\rho)$.

3.3 Cell distribution process model

For the design of the cell distribution observer the model equations (1) are discretized in the mass domain. The partial derivative is approximated using a first–order upwind finite difference scheme and the integral term representing cell birth and the first moment of the cell distribution density function is approximated by the trapezoidal rule. The discretized model equations then read

$$\begin{aligned}\dot{n}_i = &-\frac{1}{\Delta_m}\bar{\rho}(s,\epsilon)(m_i n_i - m_{i-1}n_{i-1}) - \Gamma(m_i,s,\epsilon)n_i \\ &- Dn_i + 2\Delta_m \sum_{j=i+1}^{z} \Gamma(m_j,s,\epsilon)p(m_i,m_j)n_j \qquad \text{(16a)}\end{aligned}$$

$$\dot{s} = -\bar{\rho}(s,\epsilon)\Delta_m \sum_{i=1}^{z} m_i n_i - D(s - s_{\text{in}}) =: f_s(\boldsymbol{x}) \qquad \text{(16b)}$$

$$n_{z+1} = 0, \quad n_i(0) = n_{i,0}, \quad s(0) = s_0\,, \qquad \text{(16c)}$$

where the discretization step size is given by Δ_m, the cell density of mass m_i at time t is denoted by n_i, and z is the number of interior discretization points. Introducing the state vector $\boldsymbol{x}_n = [\boldsymbol{n}^T, s]^T = [n_1, ..., n_z, s]^T$ equations (16) can be re–cast into the form

$$\dot{\boldsymbol{x}}_n = \boldsymbol{f}(\boldsymbol{x}_n) = \begin{bmatrix}\boldsymbol{A}(s,\epsilon)\boldsymbol{n} \\ f_s(\boldsymbol{x}_n)\end{bmatrix}, \; \boldsymbol{x}_n(0) = \boldsymbol{x}_{n,0} \in \mathbb{R}^{z+1}_{\geq 0}\,, \qquad (17)$$

where $\boldsymbol{A}(s)$ is constructed from (16a) and has a triangular matrix structure with additional elements on the first lower off diagonal

$$\boldsymbol{A}(s,\epsilon) = \bar{\rho}(s,\epsilon)\begin{bmatrix} * & * & * & * & \cdots & * & * & * \\ * & * & * & * & \cdots & * & * & * \\ 0 & * & * & * & \cdots & * & * & * \\ 0 & 0 & * & * & \cdots & * & * & * \\ \vdots & \vdots & \vdots & \vdots & \vdots & \vdots & \vdots & \vdots \\ 0 & 0 & 0 & 0 & \cdots & 0 & * & * \end{bmatrix}. \qquad (18)$$

Note that the boundaries of the cell distribution n_0 and n_{z+1} can be excluded from the state vector, because of the containment conditions $\bar{\rho}(s,\epsilon)m_* = 0$ and $n_{z+1} = 0$. The analysis of the observability property of each subsystem considering total biomass measurements is addressed in the next section.

4. OBSERVABILITY ANALYSIS OF THE ESTIMATION PROBLEMS

In the previous sections the considered optimal control problem is addressed using three estimation problems. One given by estimating the gradient with respect to the input and measuring an unknown cost function, another given by estimating possible uncertainties in the growth dynamics and the third by estimating the cell density distribution. Thus the fundamental question arises about the observability property of each considered problem, which gives insight about the observer dynamics, i.e., about the stabilization of the estimation error dynamics.

4.1 Observability of the gradient estimation

In the previous section two process models for the gradient estimation are derived. Note that these are given by the nonlinear time–varying dynamics (13) and (14) and that both models only differ in the demodulation by means of the dither signal. The linearization of the observability map of (13) for the measurement equation (9) reads

$$\frac{\partial}{\partial \boldsymbol{x}}\mathcal{O}(\boldsymbol{x}) = \frac{\partial}{\partial \boldsymbol{x}}\begin{bmatrix} x_1 \\ x_2(kx_2 + d)\end{bmatrix} = \begin{bmatrix} 1 & 0 \\ 0 & 2kx_2 + d\end{bmatrix}$$

which is of full rank and thus locally observable as long as $2kx_2 + d \neq 0$ holds true.

Considering (14) and (9) one obtains

$$\frac{\partial}{\partial \boldsymbol{x}}\mathcal{O}(\boldsymbol{x}) = \begin{bmatrix} 1 & 0 \\ 0 & 2kx_2 + \dot{d}\end{bmatrix} \qquad (19)$$

which is of full rank as long as $2kx_2 + \dot{d} \neq 0$ holds true.

It is important to note that both process models are not globally observable. Especially close to the optimality condition, where $x_2 \approx 0$ holds true, the observability property relies only on the dither signal. To avoid poor conditioning, the dither signal should be chosen such that $2kx_2 + d$ or $2kx_2 + \dot{d}$ are large for most times. Is the dither signal given by a classical sine wave, one obtains

$$d = \alpha_d \sin(\omega_d t), \quad \dot{d} = \alpha_d \omega_d \cos(\omega_d t)$$

with the amplitude α_d and angular frequency ω_d. It can be seen that in case of (14) ω_d can serve as a design parameter to address the conditioning, i.e., for $\omega_d \gg 1$ conditioning is enhanced, whereas for $\omega_d \ll 1$ the matrix in (19) might be poor conditioned. Nevertheless, arbitrary values for ω_d can generally not be assigned in the proposed extremum seeking approach due to a required separation of the time scales of the excitation and the system dynamics. Since local observability is lost at specific points and times (due to d being time–variant) an optimization based observer approach like the Kalman filter and its extensions for nonlinear system is proposed (see, e.g., Lewis et al. (2017)) for the estimation problem, instead of an observer design approach relying on the inverse of the observability map.

4.2 Observability of the uncertainties in the growth rate

The linearization of the observability map of system (15) reads

$$\frac{\partial}{\partial \boldsymbol{x}_b}\mathcal{O}(\boldsymbol{x}_b) = \begin{bmatrix} 1 & 0 & 0 \\ \bar{\rho}(s,\epsilon) - D & \frac{\partial}{\partial s}\bar{\rho}(s,\epsilon)b & \frac{\partial}{\partial \epsilon}\bar{\rho}(s,\epsilon)b \\ \mathcal{O}_{31} & \mathcal{O}_{32} & \mathcal{O}_{33}\end{bmatrix}$$

with $\mathcal{O}_{31}$, $\mathcal{O}_{32}$, and $\mathcal{O}_{33}$ given by

$$\mathcal{O}_{31} = (\bar{\rho} - D)^2 + \left(\frac{\partial}{\partial s}\bar{\rho}\right)[D(s_{\text{in}} - s) - 2b\bar{\rho}]$$

$$\mathcal{O}_{32} = b\left[\left(\frac{\partial}{\partial s}\bar{\rho}\right)(2\bar{\rho} - 3D) + \left(\frac{\partial^2}{\partial s^2}\bar{\rho}\right)\dot{s} - b\left(\frac{\partial}{\partial s}\bar{\rho}\right)^2\right]$$

$$\mathcal{O}_{33} = b\left[2\left(\frac{\partial}{\partial \epsilon}\bar{\rho}\right)(\bar{\rho} - D) + \left(\frac{\partial}{\partial \epsilon \partial s}\bar{\rho}\right)\dot{s} - b\left(\frac{\partial}{\partial s}\bar{\rho}\right)\left(\frac{\partial}{\partial \epsilon}\bar{\rho}\right)\right]$$

where the dependency of $\bar{\rho}(s,\epsilon)$ is not indicated for the sake of clarity. It can be seen that rank loss occurs when $\mathcal{O}_{32} = \mathcal{O}_{33} = 0$ holds. Clearly, this is the case when no biomass is in the reactor, i.e. $b = 0$. It is also worth to point out that D is given by the proposed extremum seeking control scheme, such that a continuous excitation by means of the dither signal d is applied. Nevertheless, since the performed analysis is only local an optimization based observer scheme is considered.

Note that there is no interconnection between the considered estimation problems so far. Clearly, the actual value of ϵ has also an impact on the actual value of $\nabla_u J(u)$ but the knowledge of ϵ is not required in the control scheme such that the gradient estimation is independent of the reactor model.

4.3 Observability of the cell population balance model

Finally, the observability property of system (16) and the measurement equation (6) is discussed. Note that the structural observability of this system without any uncertainties, i.e., $\epsilon = 0, \forall t > t_0$ is addressed in Jerono et al. (2021a) revealing local structural observability in batch operation $(D = 0)$ as long as $s \neq 0$ holds. For the special case of equal cell partitioning, $z = 2$ and $s \gg K_s$ the existence of indistinguishable trajectories can be excluded, which is shown in Jerono et al. (2023). Nevertheless, having uncertainties in the growth rate, the estimation of the cell population distribution cannot be decoupled from the estimation of the uncertainties ϵ, leading to a cascaded structure of these two estimation problems. Technically, the model (16) considering the growth dynamics (8) lead to a nonlinear time–varying system due to the time–varying parameter ϵ, which is estimated by the other observer. Because the analysis of such systems in high dimensions is cumbersome, the observability property discussed here is also in a structural manner. Note that the specific structure of the model can be written in terms of (17) and (18). Noting that the measurement in terms of trapezoidal rule reads

$$y = \int_{m_*}^{m^*} mn(m,t)\mathrm{d}m \approx \Delta \sum_{i=1}^{z} m_i n_i \,, \tag{20}$$

the same network graph as in Jerono et al. (2021a) is obtained with the only difference given by the fact that, here, the growth dynamics are changing with time. Nevertheless, since the structural analysis is restricted to state interconnections, which are non–zero, the same structural result is obtained as long as $\bar{\rho}(s,\epsilon) \neq 0$. This also means that, as in the previous subsections, the (structural) observability cannot be ensured for the general case, so that an optimization based observer, like the extended Kalman filter, is also designed for this estimation problem.

5. SIMULATION RESULTS

Table 1. Parameter list

Parameter	Value	Unit	Parameter	Value	Unit
k_s	1	h^{-1}	z	50	–
K_s	0.2	g/l	q	5	–
ω_ϵ	0.0105	rad/h	β_ϵ	0.001	1/h
s_{in}	1	g/l	α_d	0.01	1/h
m_*	0	g	ω_d	0.2	rad/h
m^*	$1.5 \cdot 10^{-11}$	g	$q_{b,b}$	0.01	$\mathrm{g}^2/\mathrm{l}^2/\mathrm{h}$
β	$1.21 \cdot 10^{-3}$	–	$q_{b,s}$	0.01	$\mathrm{g}^2/\mathrm{l}^2/\mathrm{h}$
r_m	10^{-6}	$\mathrm{g}^2/\mathrm{l}^2$	$q_{b,\epsilon}$	0.6	$1/\mathrm{h}^3$
$q_{g,1}$	10^{-4}	$\mathrm{g}^2/\mathrm{l}^2/\mathrm{h}^3$	$q_{g,2}$	0.1	$\mathrm{g}^2/\mathrm{l}^2/\mathrm{h}^4$

Based on the analysis of the previous sections the proposed control strategy and estimations by means of extended Kalman filters is tested in simulations. The Kalman filters are designed with a continuous correction scheme, given that the growth dynamics of bioprocesses are usually much slower than the sampling time of online biomass sensors. The corresponding simulation and tuning parameters are listed in Table 1, where r_m is the covariance of measurement noise and q_b and q_g represent the tuning parameters of the Kalman filters for the uncertainty and gradient estimation, respectively. The uncertainty ϵ is chosen to be given by a sine wave with the amplitude a_ϵ and radial frequency ω_ϵ, which is added to a ramp function of slope β_ϵ in the time interval $t \in [200\,\mathrm{h}, 700\,\mathrm{h}]$ (see also Fig. 2 bottom–left). The tuning parameters of the Kalman filter for the cell distribution estimation are given by

$$q_{n,i,i} = k_q \frac{1}{\sqrt{2\pi\sigma^2}} e^{\left(-\frac{(m_i - m_q)^2}{2\sigma^2}\right)}, \quad i \in \{1, \ldots, z\}\,,$$

which represents a scaled and shifted Gaussian distribution with $m_q = 4.326 \cdot 10^{-11}$, $\sigma = 1.8 \cdot 10^{-11}$ and $k_q = 3.161 \cdot 10^{27}$ and is based on the consideration that close to the boundaries of $m \in [m_*, m^*]$ model (16) is assumed to be more accurate than in between. The results of estimating the uncertainty in the growth rate is presented in Fig. 2. The estimations are given by dashed red lines and the true values are marked blue. On the left side the estimations over the whole cultivation period of 1000 h are shown, whereas the right side shows the initial convergence behavior. It is important to note that although no initial error in the uncertainty is assumed, the estimation is faulty within the first 20 hours, which is due to initial errors in the substrate and total biomass concentration. From an experimental perspective, the initial errors can be avoided by a preceded batch experiment. Nevertheless, to illustrate the

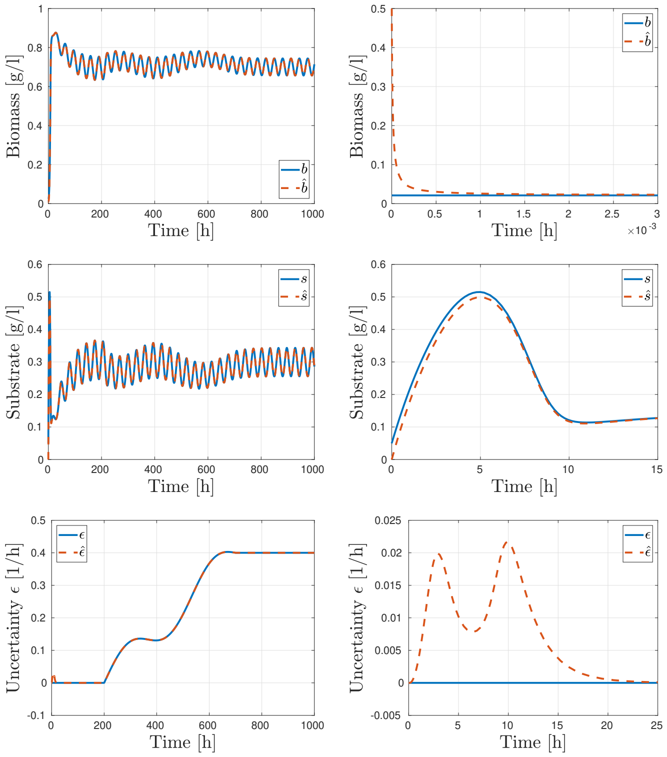

Fig. 2. Simulation results of the uncertainty estimation. True trajectories (blue) and estimated trajectories (dased red) for $t \in [0\,\mathrm{h}, 1000\,\mathrm{h}]$ (left) and initial convergence (right).

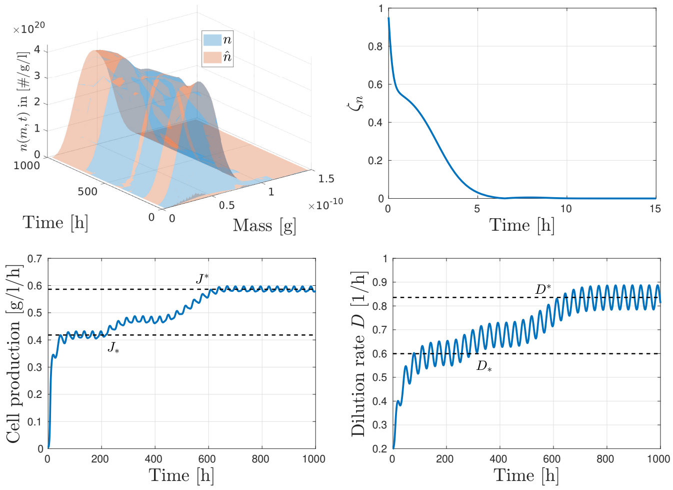

Fig. 3. Simulation results of cell distribution estimation and extremum seeking controller. True values (blue), estimated values (red) and optimal operation points before and after change in growth (dashed black).

convergence behavior initial errors are considered in the simulations. Note that the substrate concentration and the uncertainty are well estimated over the whole experiment. Fig. 3 shows the estimation of the cell distribution density function and the performance of the proposed extremum seeking control scheme for maximizing the cell production rate. To evaluate the convergence behavior of the cell distribution estimation a normalized approximation of the L^1–norm by means of

$$\zeta_n(t) = \frac{1}{\int_{m_*}^{m^*} n(m,t)\mathrm{d}m} \int_{m_*}^{m^*} |n(m,t) - \hat{n}(m,t)|\mathrm{d}m$$

in the time interval of $t \in [0\,\mathrm{h}, 15\,\mathrm{h}]$ is shown. It can be seen that the estimation error $\zeta_n(t)$ converges within the first 5 hours.

For a validation of the optimality with respect to the cell production rate the corresponding (constant) optimal inputs D and related objective function values J are highlighted dashed black before and after the considered changes in the growth rate by means of ϵ with D_* and D^*, as well as J_* and J^*, respectively. Note that these values can be obtained by bifurcation analysis. It can be seen that proposed control scheme is capable of maintaining optimality in the simulations despite the considered uncertainties.

6. CONCLUSION

In this work the optimal control problem of maximizing the cell production rate in chemostat reactors under possibly time–varying uncertainties in the growth rate is addressed. The optimal control problem is addressed using three estimation problems. For each subsystem the observability property is investigated revealing that local observability cannot be ensured for all time instances due to the time–varying behavior of the uncertainties and the dither signal. Based on these results three extended Kalman filters are designed for the estimation of the gradient with respect to the input, uncertainties in the growth rate and the cell mass distribution density function based on biomass measurements. The estimation and control performance is tested in simulations showing that optimality can be preserved in the presence of time–varying uncertainties.

REFERENCES

Ariyur, K.B. and Krstic, M. (2003). Real-time optimization by extremum-seeking control. John Wiley & Sons.

Ferenci, T. (2007). Bacterial physiology, regulation and mutational adaptation in a chemostat environment. Advances in microbial physiology, 53, 169–315.

Gelbert, G., Moeck, J.P., Paschereit, C.O., and King, R. (2012). Advanced algorithms for gradient estimation in one-and two-parameter extremum seeking controllers. Journal of Process Control, 22(4), 700–709.

Guay, M. and Dochain, D. (2015). A time-varying extremum-seeking control approach. Automatica, 51, 356–363.

Guay, M., Dochain, D., and Perrier, M. (2004). Adaptive extremum seeking control of continuous stirred tank bioreactors with unknown growth kinetics. Automatica, 40(5), 881–888.

Jerono, P., Schaum, A., and Meurer, T. (2021a). Moment-based kalman filter design for cell population balance models in batch fermentation processes. IFAC-PapersOnLine, 54(3), 19–24.

Jerono, P., Schaum, A., and Meurer, T. (2021b). Parameter identification of a yeast batch cell population balance model. IFAC-PapersOnLine, 54(7), 144–149.

Jerono, P., Schaum, A., and Meurer, T. (2022). Feedforward and output–feedback control of the cell distribution in chemostat yeast fermentations. IFAC-PapersOnLine, 55(7), 556–561.

Jerono, P., Winkin, J., Wouwer, A.V., and Schaum, A. (2023). Indistinguishability analysis and observer design for size-structured cell populations. IFAC-PapersOnLine, 56(2), 581–586.

Kurth, A.C., Schmidt, K., and Sawodny, O. (2021). Inversion-based and optimal feedforward control for population dynamics with input constraints and self-competition in chemostat reactor applications. J. Dyn. Sys., Meas., Control, 143(5).

Leblanc, M. (1922). Sur l'electrification des chemins de fer au moyen de courants alternatifs de frequence elevee. Revue générale de l'électricité, 12(8), 275–277.

Lewis, F.L., Xie, L., and Popa, D. (2017). Optimal and robust estimation: with an introduction to stochastic control theory. CRC press.

Lutz, M., Freudenthaler, G., Roduner, C., and Meurer, T. (2019). Ukf-based constrained extremum-seeking control with application to a large-bore gas engine. In 2019 IEEE 58th Conference on Decision and Control (CDC), 561–566. IEEE.

Mantzaris, N.V. and Daoutidis, P. (2004). Cell population balance modeling and control in continuous bioreactors. Journal of Process Control, 14(7), 775–784.

Ramkrishna, D. and Singh, M.R. (2014). Population balance modeling: current status and future prospects. Annual review of chemical and biomolecular engineering, 5(1), 123–146.

Sharifian, M. and Fanaei, M.A. (2008). Nonlinear control of a continuous bioreactor based on cell population model. In WCSET 2008.